

Crack arrest through branching at curved weak interfaces: an experimental and numerical study

M.T. Aranda^a, I.G. García^a, J. Reinoso^a, V. Mantič^a, M. Paggi^b

^a*Grupo de Elasticidad y Resistencia de Materiales, Escuela Técnica Superior de Ingeniería, Universidad de Sevilla
Camino de los Descubrimientos s/n, 41092 Sevilla, Spain*

^b*IMT School for Advanced Studies Lucca, Piazza San Francesco 19, 55100, Lucca, Italy*

Abstract

The phenomenon of arrest of an unstably-growing crack due to a curved weak interface is investigated. The weak interface can produce the deviation of the crack path, trapping the crack at the interface, leading to stable crack growth for certain interface geometries. This idea could be used as a technical solution for a new type of crack arrester, with a negligible impact on the global stiffness, strength and weight of the structure. In order to exploit this concept, an experimental campaign based on photo-elasticity and digital image correlation is carried out, showing the capability of curved weak interfaces to arrest cracks. The experiment is repeated for several geometrical configurations through the modification of the interface curvature radii. The phenomenon of crack deviation and subsequent arrest at the interface is also investigated with the assistance of a computational model based on the finite element method. The computational predictions provide the rationale for the interpretation of the experimental observations, and distinguish between the different behaviour of concave and convex interfaces. Consequently, as is shown in the present study, the curved interface concept fosters new routes for the attainment of structures with enhanced fracture resistance capacities, which are of paramount importance for materials and components used in extreme conditions.

The final version of this manuscript has been published in Theoretical and Applied Fracture Mechanics Volume 105, February 2020, 102389.

Keywords: Curved interface, Crack arrest, Fracture mechanics, Experimental mechanics, Crack-interface interaction, Crack branching

1. Introduction

The damage-tolerant approach has become a recurrent standard for the design of structures in aerospace and ship-building industries, among others, see e.g. [1]. The objective of this methodology is the specific design of structures tolerant to the presence of flaws, i.e. where the presence of cracks does not imply necessarily the catastrophic failure of the structure upon their propagation. Following this idea, many attempts have been made in materials science in order to identify optimal material microstructures to arrest cracks, also inspired by nature, see e.g. [2, 3, 4, 5]. However, the application of this approach generally requires: (i) advanced inspection techniques in order to detect damage events prior they reach the corresponding critical sizes, and (ii) the design of structural elements that enable either preventing or slowing-down the progress of crack evolution and the related structural softening. Within this context, the so-called crack arresters can be understood as structural elements that are designed for this purpose. In the last years, such a concept has been prolifically employed in different practical applications in engineering, see e.g. [6, 7]. In materials science, the role of structural arresters can be played by material interfaces, suitably arranged across the scales in order to prevent the catastrophic propagation of flaws. For instance, [5] have shown that a two-scale arrangement of material interfaces can be profitable to

Email addresses: maranda2@us.es (M.T. Aranda), israelgarcia@us.es (I.G. García), jreinoso@us.es (J. Reinoso), mantic@us.es (V. Mantič), marco.paggi@imtlucca.it (M. Paggi)

stop the propagation of cracks from the microscale to the mesoscale in polycrystalline materials used for extreme structural applications such as drilling.

With the aim of exploiting the role of material interfaces, we consider here weak interfaces, which are material discontinuities favorable to debond and deviate cracks by investigating their curvature. It is in fact well-known from the fundamental studies by [8, 9] that the competition between crack branching and penetration when a crack impinges into an interface can lead to different scenarios, such as crack penetration, single deflection along the interface, and also double deflection, depending on the elastic mismatch between the two joined materials and the toughness of the interface as compared to that of the bulk. Those results, however, were restricted to flat interfaces, while interfaces with curvatures could also be explored and manufactured. The sustained interest emerges from characteristic material disposals in many engineering systems, ranging from composite materials, presence of bonding lines, curved fibers, among many other scenarios. Therefore, the profound understanding of crack propagation at interfaces can be conceived as a key aspect that can actively contribute to the design of new generation of composite materials and structures with enhanced fracture resistance properties.

Reference studies in this context can be traced back to [10], who established a strength-based criterion to determine the potential crack path through the stress field estimations near the crack tip recalling the [11] procedure. Posterior investigations advocated the use of linear elastic fracture mechanics (LEFM), which exploited an energetic approach to predict crack penetration vs. crack deflection scenarios in multi-material systems. LEFM-based procedures generally require the computation of the ERRs corresponding to a perturbation of the linear elastic solution by introducing infinitesimal kinks associated with crack penetration or crack deflection, see [9, 12, 13, 14]. These contributions have been of notable interest to many researchers in order to interpret many experimental data, pinpointing the necessity of developing reliable numerical and theoretical procedures in order to achieve a more thorough comprehension of such phenomena.

Subsequently, from a computational standpoint, notable works have been conducted through the use of the so-called cohesive zone model (CZM) to predict penetration vs. deflection scenarios. The fundamentals of the CZM were originally proposed in [15] and [16], who considered a combined strength-and-energy approach to trigger fracture events in solids. Within this context, [17] analyzed these phenomena using the CZM in media with the presence of weak interfaces, showing that the fracture toughness and the strength of the bulk and of the interface play a significant role in order to determine whether the crack will deflect along the prescribed interface or, conversely, it will propagate into the adjacent body. Specifically, it has been addressed that higher interface strength promotes crack penetration, whereas weak interfaces induce crack deflection along existing interfaces, examining a situation where the interface is perpendicular to the traveling mother crack. However, one of the main limitations of the CZM relies on the fact that: (i) it implies the pre-definition of the potential crack paths prior running the simulations, in its implicit version [18], or (ii) it requires the incorporation of complex crack tracking algorithms using the explicit CZM, confining the potential crack paths to the boundaries of the corresponding discretization [19] (mostly in the spirit of the finite element method, FEM). In contrast to the previous computational methodology, the advent of the phase field method (PFM) of fracture [20, 21], which is based on the regularization of the variational formulation of brittle fracture due to [22], does offer a potent modeling alternative with strong potential for simulating very complex fracture phenomena. With respect to heterogeneous media, [23] devised the consistent coupling of the PFM with the CZM (PF-CZM) which is especially oriented to the simulation of fracture events with the presence of weak interfaces. The predictive capabilities of the seminal approach developed in [23] has been shown through its application in layered ceramics [24], laminates [25], polycrystalline materials [26], and micro-mechanics of composites [27], retrieving also fundamental results from LEFM [9] concerning bi-materials systems.

A plausible alternative methodology to the previous procedures is the so-called Coupled Criterion (CC) [28] or Finite Fracture Mechanics (FFM), whose rigorous development implied the simultaneous satisfaction of the corresponding energy- and strength-based criteria with excellent accuracy capabilities. CC-based method permits to gain a plausible insight into the physical events under investigation yielding to persuasive explanations with the precise application of both strength and energy criteria. The application of the CC or FFM has successfully applied in many engineering problems [29], material bonding [30], thermo-mechanical studies [31, 32] and more specifically within the context of laminate composite materials [33, 34], among many others.

From the previous brief review, it becomes evident that the investigation of the competition between crack deflection and propagation at weak interfaces has been long identified as one of the topics that has attracted a great deal of research in the last years. Comprehensive experimental studies have investigated the problem of interfacial crack growth [35, 36]. Thorough investigation on this specific application complying layered composite materials have been conducted in [37] and by Tippur and co-authors [38]. It is also worth mentioning the development from this researcher group of new experimental techniques to trigger dynamic crack events using the a novel vision-based method denominated as Digital Gradient Sensing (DGS) which is combined with ultrahigh-speed photography [39]. Nevertheless, most of the existing studies in the related literature have been principally devoted to the analysis of straight interface definitions following either perpendicular [38] or inclined directions [37] with respect to the primary crack. However, at present, situations with the possible presence of curved and/or patterned interfaces, that yield to outstanding fracture resistance properties [40, 41, 42, 43], has received a very scarce attention. Consequently, motivated by these real scenarios, the present study is devoted to evaluate the ability of curved weak interfaces to serve as crack arresters, i.e. carefully investigating crack deflection vs. propagation in specimens with curved interfaces.

In the sequel, after a description of the experimental setup, a detailed analysis of the results and the corresponding interpretation is carried out. Thus, the manuscript is organized as follows. The experimental campaign will be presented in Section 2. The results obtained will be analyzed with the assistance of a computational model described in Section 3. The discussion of the results is included in Section 4, whereas the main conclusions are summarized in Section 5.

2. Experimental campaign

The objective of this section is to analyze the viability of the design of a special geometry of a weak interface to *retard or modify* the crack path, by means of deviating the (mother) crack along such an interface. In addition to deviate the crack, the role played by different interface curvatures onto the overall structural response are carefully investigated.

In the following, current experiments will be presented in relation to: the geometry of the specimens, their fabrication procedure and materials used, and the method and experimental setup. Finally, details regarding the experimental results for different interface curvatures and positions with respect to the mother crack will be put forward.

2.1. Specimens design and fabrication

Focusing on the study of the effect of the curvature radius of a weak interface on the propagation of a dynamic crack, appropriate specimens were designed including a novel concept of curved interface,. This interface bonds two parts of a rectangular specimen with dimensions $300 \times 50 \times 8$ mm. Two types of specimens with an initial crack and a curved interface were fabricated, namely: (i) the so-called *concave curved interfaces*, where the initial mother crack is approaching a concave (non-convex) part of specimen (i.e. approaching an interface point from the side of the osculating circle), and (ii) the so-called *convex curved interfaces*, where the initial mother crack is approaching a convex part of the specimen (i.e. approaching an interface point from the side opposite to the osculating circle), as shown in the sketch in Figure 1a. For each type of interface, different curvature radii were studied, ranging from 15 mm to 75 mm, with discrete variations of 10 mm each. Such interfaces were located tangent to the central longitudinal axis of the specimen, as shown in Figure 1b. In this way, 14 specimens were patterned, seven of them corresponding to concave interfaces and other seven configurations with convex interfaces.

The material selected for the fabrication of the specimens was polymethyl methacrylate, known as PMMA, because it is a brittle material suitable for photo-elasticity within a certain application range. Moreover, from the practical point of view, it was easy to form bonded interfaces with PMMA using commercial solvents. Note that PMMA was frequently used in previous experimental studies for interface fracture, see [44] and the references therein given. Likewise, the interface was made of a transparent, bi-component epoxy resin with a viscosity of 6.000/9.000 cps and a density of 1.10 gr/cc, a material which could also be used for photo-elasticity [45, 46, 47].

After several preliminary manufacturing and testing trials to assess the best bonding conditions, the specimens were manufactured by cutting them with a laser cutter of 150 W, splitting the specimen

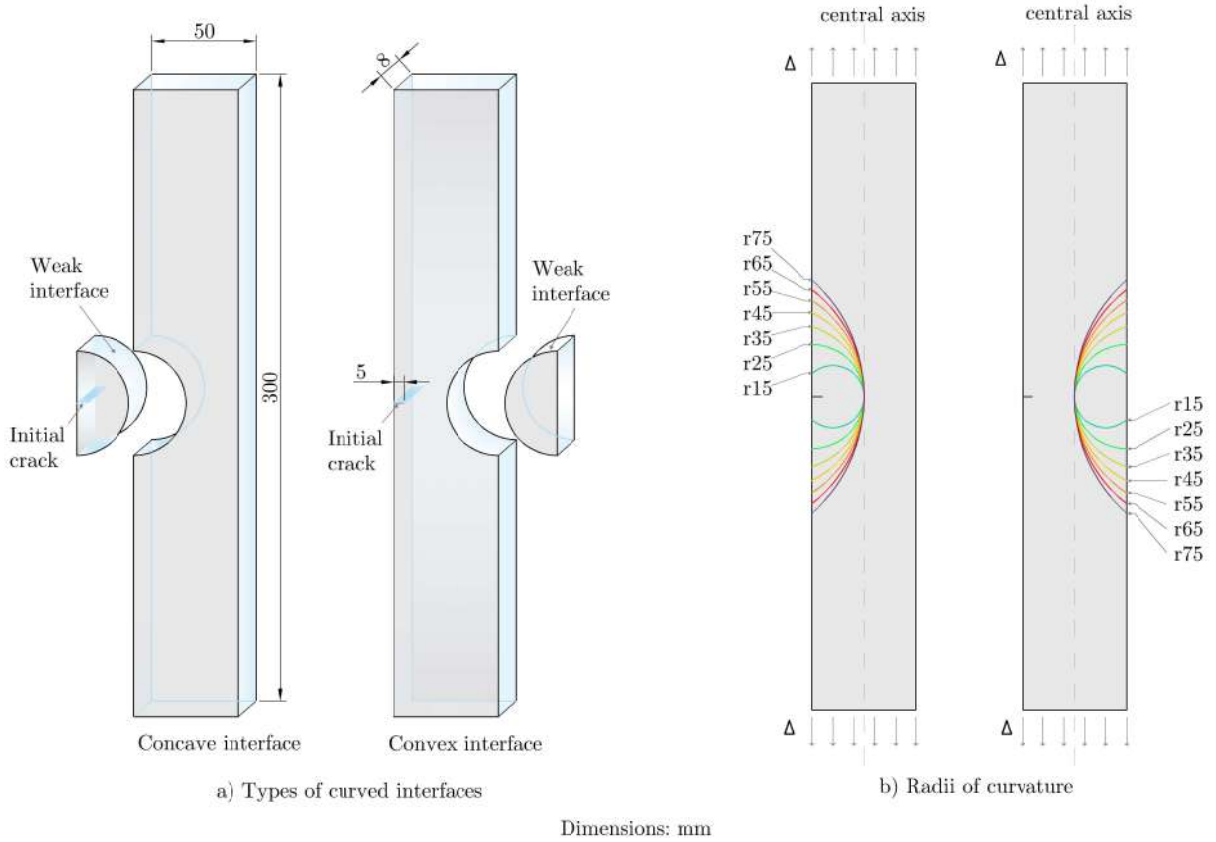


Figure 1: Sketch of the studied specimens geometry. a) Concave and convex weak interfaces. b) Different radii of curvature.

into two parts. Subsequently, an initial crack (pre-crack) of approximately 5 mm length and oriented perpendicular to the edge was introduced in each specimen by a razor blade, as recommended in [48] and already used for other experiments with the same material, see e.g. [49]. In a next stage, the specimens were prepared to bond the two parts by cleaning the contact surfaces. During this procedure, the initial mother crack was covered to prevent undesired leakage of the adhesive into it.

The two parts of the specimen were bonded together using a special fixture under controlled pressure to attain and manage the proper adhesive thickness. Then, the specimens were left curing at room temperature for a period of 6 days, in order to achieve the required bonding strength and avoid residual stresses that would affect photo-elasticity measurements. The excess of adhesive was not removed, precluding the pore formation at the interface. Finally, an adhesive drop of pipette was provided at the intersection line of the interface and the specimen edges, in order to prevent premature failure near such critical zone close to the boundaries.

2.2. Experimental setup

The experimental setup, see Figure 2, consisted of: (i) a mechanical system to apply a tensile loading on the specimen, (ii) an optical system to produce isochromatic fringe patterns to highlight the crack path during propagation, and (iii) an imaging system to record the photo-elastic fringe patterns and the specimen during crack growth.

The mechanical system involved an Instron 4482 universal testing machine, which was used to test all the specimens under monotonic tensile conditions up to failure. The testing machine was equipped with a 100 kN load cell, being the tests conducted under displacement control mode. Due to the longitudinal dimensions of the specimens, i.e 300 mm in length, they were fixed to the testing machine using a standard gripping, with negligible influence of the clamping area on the fracture process region within the coupon.

The loading application was carried out by the adoption of a uniform applied displacement of 0.5 mm/s during the tests.

The imaging system was composed of two Fastcam Mini Ax-200 monochrome high speed cameras, which are able to record images at rates up to 0.9 million frames per second (fps). In our experiments, the frequency of recording ranged from 48,000 to 160,000 fps, depending on the area observed and the resolution prescribed for the camera. Two regions of interest were defined in this study: (i) The initial mother crack and the subsequent crack path up to reaching the interface. Accordingly, one camera was focused on a strip line of 512×48 pixels region at 160,000 fps to register a detail view of the first propagation. (ii) The second region of interest, i.e. the interface location, was recorded using another camera focusing on a 384×288 pixels region to register a view at 48,000 fps. This optical method was chosen for the tests because it allowed the closest observation of the propagation of a fast running crack to be performed. To illuminate the specimen, two strong flash lamps were used, composed of 4 heads of LED lamps of high power and low consumption model QT of GSVitec.

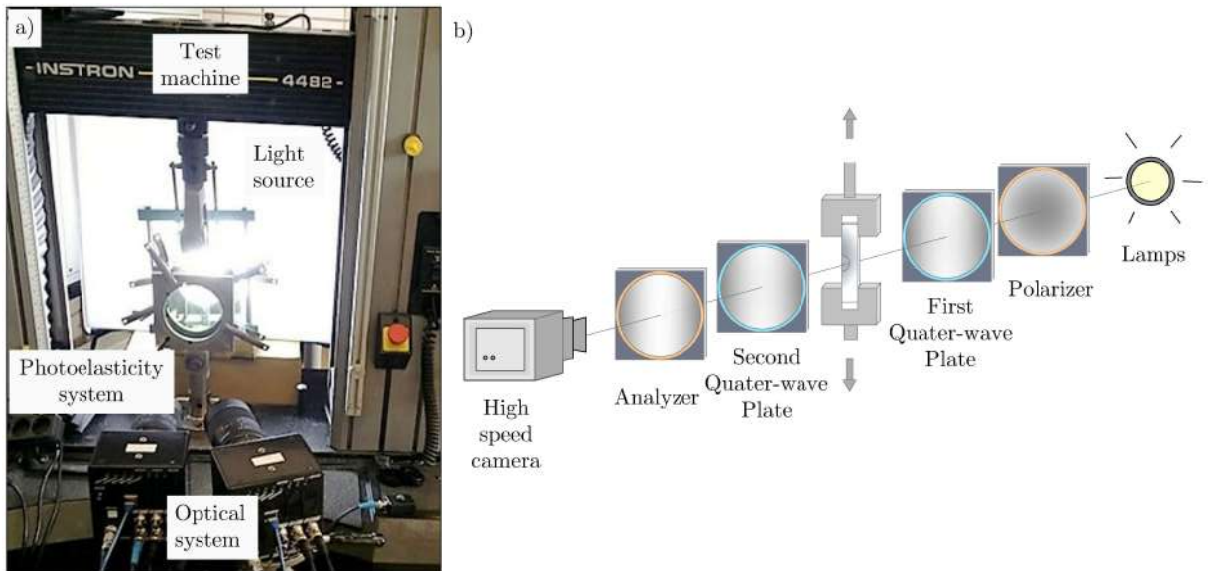


Figure 2: a) Close-up photograph of the experimental setup in this study. b) Schematic of the photo-elasticity setup.

With regard to the photo-elasticity system, the usage of this equipment has been adopted due to the fact that it permits a rapid and efficient identification of the crack trip along the propagation of the crack within the specimen. It regarded of a polarizer, an analyzer, two quarter-wave plates between which the model under testing was introduced, and a light source, see Figure 2b. Hence, the first quarter-wave plate was placed between the polarizer and the specimen, whereas the second quarter-wave plate was located between the specimen and the analyzer. Therefore, as stated above, the principal aim was to qualitatively visualize stress field during crack propagation in monochromatic colors in order to track the crack advance and detect premature debonding along the weak interface.

2.3. Experimental results

This section presents the results obtained from the experimental study with the aim of obtaining qualitative conclusions and highlighting the observed trends. The first part describes the behaviour during the tests, differentiating between convex and concave curved interfaces. The second part analyzes several series of fringe pattern pictures corresponding to a crack propagation in the material in the presence of a weak interface. Finally, photographs of fractured specimens are presented, examining the effect of the interface geometry with respect to the initial crack position.

2.3.1. General response of specimens

Figure 3 shows the load-displacement curve for a convex curved interface with 35 mm radius. In this particular load-displacement curve, the ultimate load is 3.1 kN. For this ultimate loading, a fast

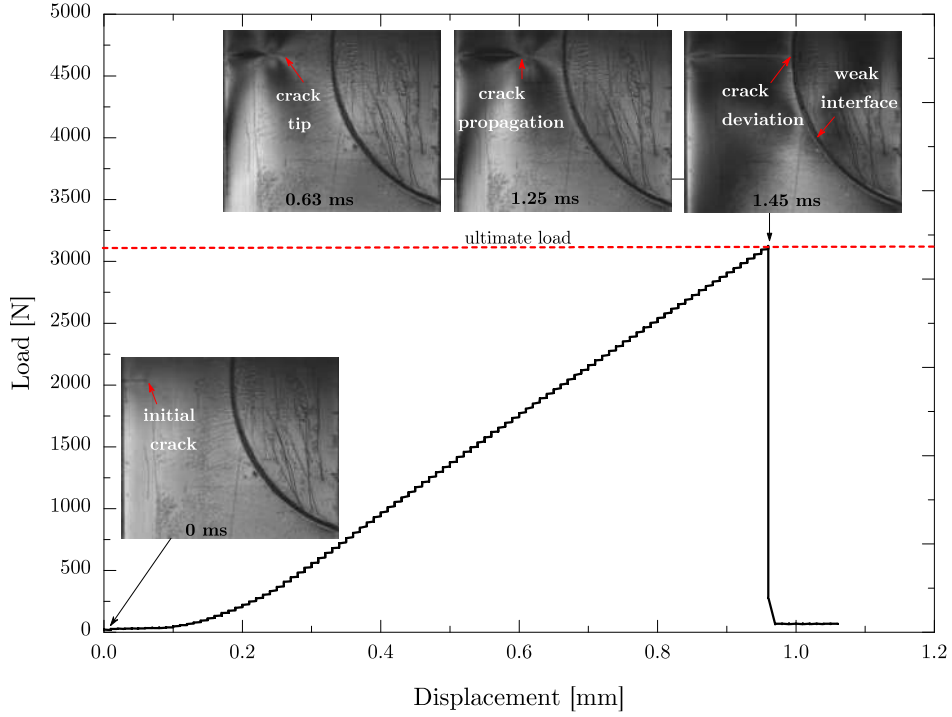


Figure 3: Load-displacement curve of the convex curved interface with a radius of curvature of 35 mm under tensile test. Magnification views of the crack and interface at the zero and the maximum load before catastrophic fracture, 48000 fps, 384×288 mm.

catastrophic crack growth can be observed in the three images shown on the top of the figure recorded at 48,000 fps. These images show a general view of crack propagation through the material until it reaches the interface, 1.45 ms after the initiation of crack propagation. At this moment, the crack is deflected towards the interface, progressing unstably through it and leading to the total failure of the specimen with a catastrophic drop in the load-carrying capacity.

For all the specimens with a convex interface, regardless their curvature radius, the same brittle response was noticed. Thus, the mother initial crack, that was generated during the manufacturing process, progressed under mode-I conditions up to reaching the interface. At this stage, this crack was trapped by the interface, and bifurcated into two interface cracks that grew simultaneously along the interface, separating the specimen into two parts. In every test, the crack extent along the interface corresponded to its entire length, so that such interface cracks did not kink out of the interface and, thus, in particular did not penetrate into the other part of the specimen. Moreover, from a qualitative standpoint of the analysis of the load-displacement evolution curve (Figure 3), it is observable that the specimens featured a quasi perfect linear elastic evolution up to an abrupt failure, at which the coupons broke in two parts.

Interestingly, in the case of concave curved interfaces, the results were drastically different. Figure 4 depicts a representative load-displacement curve for one of the specimens tested with a concave curved interface, displaying three distinct stages of crack propagation. Analyzing this plot, a first linear load-displacement branch can be observed up to the first peak load. Throughout the first stage, the mother crack propagated under mode-I conditions till reaching the interface. After the crack bifurcation at the interface, the second stage was characterized by subsequent (approximately symmetric) growth of two interface cracks, one propagating upward and the other downwards, and featuring a stable growth with an essentially steadily increasing load with some unstable jumps, as can be observed in Figure 4. In the last third stage, the final failure occurred when one crack emerges from one the the interface crack, kinking out of it towards the other part of the specimen, growing across the bulk in an unstable manner again. Note that this ultimate loading level was significantly higher than that corresponding to that

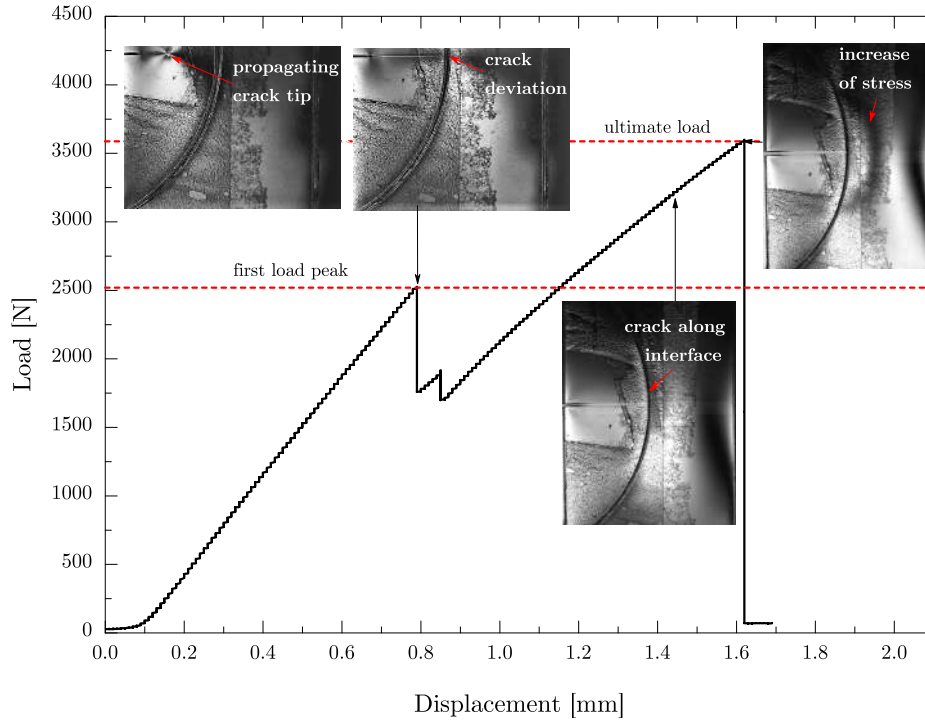


Figure 4: Load-displacement curve of the concave interface with a radius of curvature of 45 mm under tensile test. Magnification views in the first kink load point and at the ultimate load point, 48000 fps, 384 x 288 mm.

which produced the first crack propagation. This means that the presence of a concave weak interface significantly increased the load-carrying capacity of the specimen.

At this point, it is worth mentioning that the present results clearly evidenced that the interface geometry, especially its curved shape, plays a crucial role in the structural response. Thus, the insertion of a weak interface does not always produce crack penetration into the other part of the body. Therefore, the location and shape of such an interface within a given specimen and for some loading conditions may influence the creation of new daughter cracks, as discussed in the following.

2.3.2. Analysis of fringe patterns and fractured specimens

Figure 4 shows a set of images corresponding to the first peak load, showing the propagation of the initial crack until it impinges on the weak interface. From this point on, the propagation of the crack along the interface can be tracked. In these images, it can be observed that a part of the interface remains bonded and the region enclosed by the interface and mother crack flanks is unloaded. Thus, to break the other load-bearing part of specimen, including stress singularities at the interface-crack tips and a stress concentration in its net cross-section at the already broken interface, it is necessary a significant load increase, as discussed previously.

Figure 5 and Figure 6 depict a set of detailed images with the sequence of the initial propagation of the mother crack. The set of images was taken with the optical equipment at 160,000 fps. The red vertical line at the center of each image has been drawn to visually identify the interface position.

In the convex-interface configuration, Figure 5, the isochromatic lines are continuous through the interface up to 1.25 ms, just before the crack reaches the curved interface at 1.44 ms. This continuity is an evidence of the fact that the interface is perfectly bonded. After that, crack is deflected along the interface and the specimen is separated into two parts ($t = 2.44$ ms).

In the concave-interface configuration, Figure 6, the propagation of the mother crack is shown for $t = 0.56$ ms, $t = 0.75$ ms, 0.94 ms, 1.19 ms and 1.31 ms, observing a continuity of the isochromatic lines again through the interface. At $t = 1.50$ ms, the crack is deflected at the interface. Afterwards, the crack follows the path imposed by the weak interface ($t = 1.56$ ms and 2.94 ms).

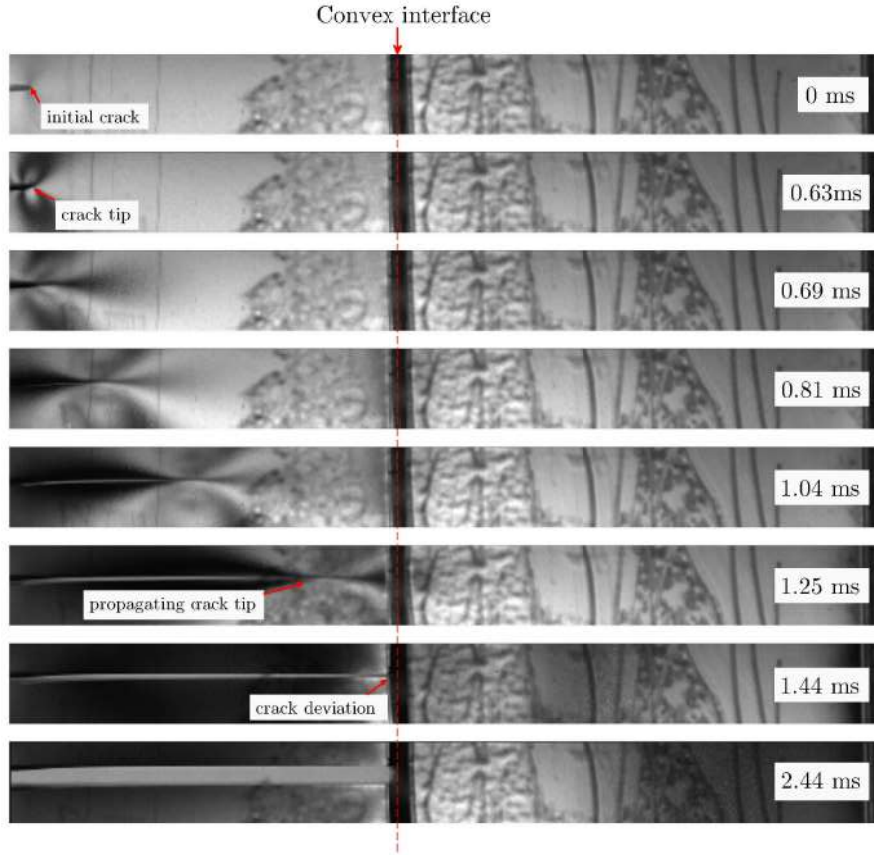


Figure 5: Series of dynamic photoelastic images of crack propagation for a 35 mm radius weak convex interface.

To assess the interface debonding, the digital image correlation (DIC) technique was also employed. A random speckle pattern was sprayed over the specimen surface, and the corresponding images were acquired before and after the fracture event. Figure 7 shows the map of the vertical strain for a concave-interface specimen. It should be emphasized that during the propagation of the mother crack there is a continuity of strain across the interface, which indicates perfect bonding. Thereby, the specimen behaved as a single homogeneous material until the crack impinged on the interface and deflected along it. After that, it is possible to observe where a discontinuity in the vertical strain field took place, which allows detecting the crack tip positions of the deflected cracks.

Finally, a post-mortem analysis of the specimens was carried out, studying the crack path in detail for each configuration under analysis. In particular, it is interesting to verify how the crack trajectory was altered by the effect of interface geometry. Typical pictures of two fractured samples, one for each configuration (convex or concave interface), are shown in Figure 8. In both cases, it is evident that the crack propagated similarly until it reached the interface and then it branched into two daughter cracks travelling along the interface. At a certain point, crack paths differed from each other. For the concave interface configuration, one daughter crack kinked out of the interface into the adjacent part. However, such branching was not observed for convex interfaces. The extent of the interface crack growth, given by the polar angle where the crack kinked out of the interface towards the other part of specimen, varied with the interface curvature radius, as detailed in Table 1.

Figure 8a shows the crack path for the convex interface configuration. A straight crack path is observed until the crack impinges on the weak interface, where it deflected and propagated trapped at the interface. After the corresponding tests, it was examined that the interface in these configurations was totally debonded, without any kinking out of the interface. Figure 8b shows the crack path for the concave interface configuration, where the dynamically growing straight mother crack deflected at the interface, where the daughter interface cracks were trapped for a while, eventually one of them kinked

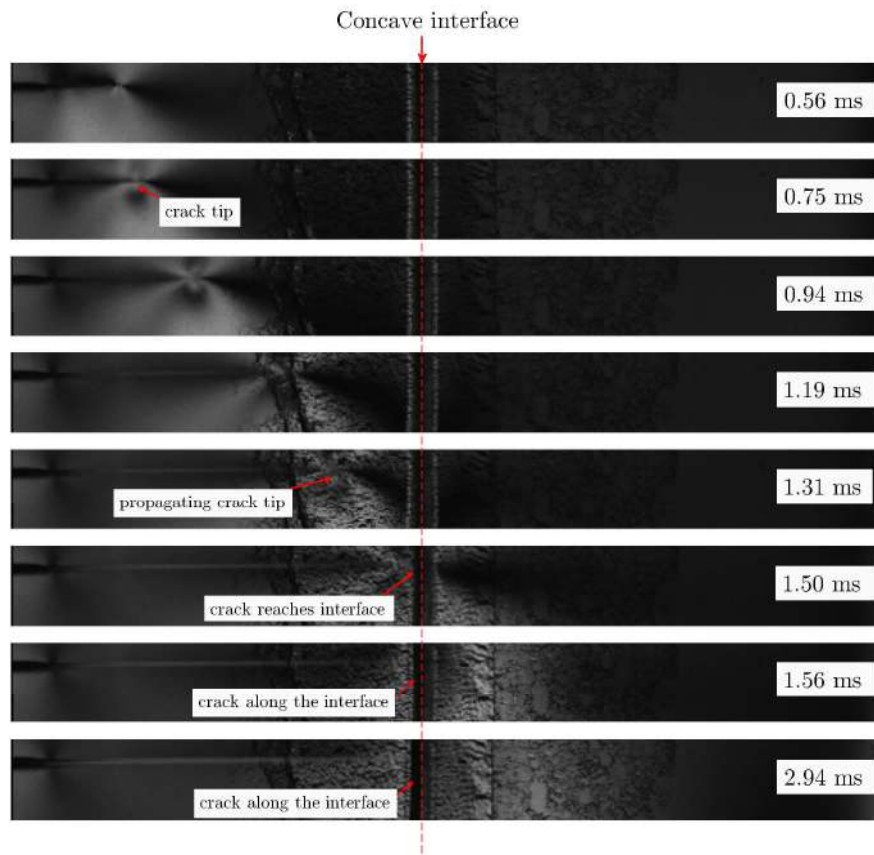


Figure 6: Series of dynamic photoelastic images of crack propagation for a 45 mm radius weak concave interface.

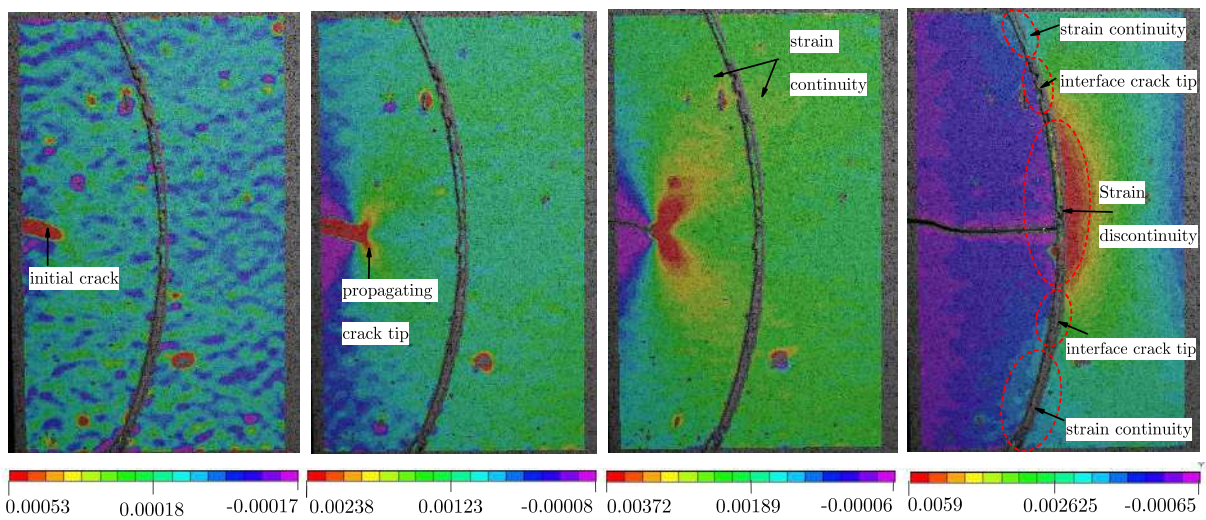


Figure 7: 2D digital image correlation representing vertical strain during crack propagation. The discontinuity of strain allows identifying the crack tip positions of the deflected cracks.

out of the interface penetrating into the adjacent bulk as a locally mixed-mode daughter crack, as shown in Figure 8.

Table 1 presents a summary of the behaviour observed in each specimen. It is interesting to notice

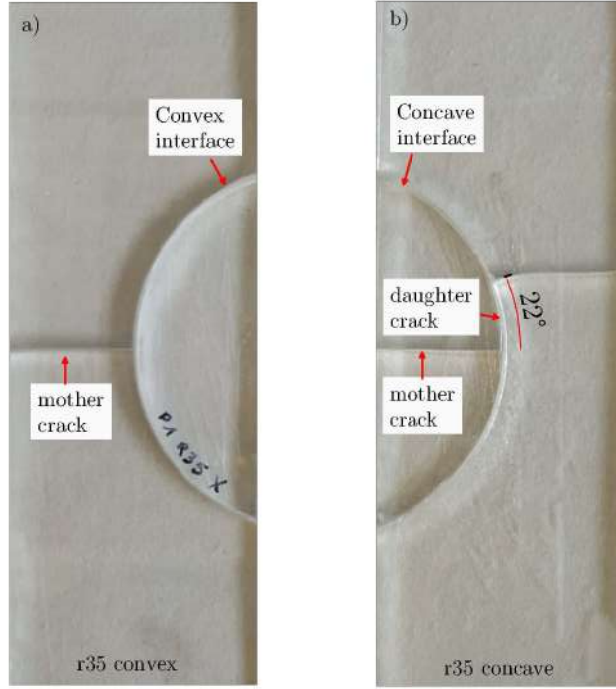


Figure 8: Photographs of fractured specimens, showing crack path in a) convex and b) concave interface configurations.

CONVEX										
Curvature radius	15 mm	25 mm		35 mm	45 mm	55 mm		65 mm	75 mm	
Specimen	S1	S1	S2	S1	S1	S1	S2	S1	S1	S2
Behaviour	unstably	unstably	unstably	unstably	unstably	unstably	unstably	unstably	unstably	penetration
CONCAVE										
Curvature radius	15 mm	25 mm		35 mm	45 mm	55 mm		65 mm	75 mm	
Specimen	S1	S1		S1	S1	S1		S1	S1	
Behaviour		arrest		arrest	arrest	arrest		arrest	penetration	
Kinking angle		25°		22°	16°	15°		18°		

Table 1: Summary of the behaviours found in each specimen. Penetration: crack grows straight across the interface. Arrest: crack deflects at the interface and it is arrested at some point of the interface. Unstably: crack deflects at the interface and grows unstably along the whole interface. Kinking angle: polar angle measured along the interface between the impinging and kinking points, see Figure 8.

that the crack was deviated for all the specimens except for those with the largest radii which failed due to crack penetration, for both concave and convex interface configurations. Thus, it appears that even a small perturbation of the interface planarity (flatness) is enough to lead to symmetric crack deflection at the interface as the preferential path. Focusing on the specimens where deflection occurred, crack growth was arrested at some point of the interface in the case of concave interface configurations. In contrast, for specimens with convex interfaces, complete debonding of the whole interface took place in an unstable manner without any crack arrest.

From the results presented in this section, it can be concluded that the curved shape of the interface dictated the crack path selection and the fracture behavior. This fact clearly shows that the introduction of a curved interface within the given specimen geometry can deflect a mother crack and also arrest it.

3. Computational analysis

The main focus of this section is to provide a possible interpretation based on LEM concepts of the previous experimental results presented in Section 2. To this aim, we use a computational model based on the finite element method. To double check the present computational results, in addition to a

mesh convergence study (not presented here for the sake of brevity), these results are compared, where possible, to the predictions obtained by using the well-known empirical formulas available in fracture mechanics handbooks. Moreover, some limit predictions obtained by a semi-analytical method available in the literature are compared with the present computational results.

3.1. Numerical model

The proposed model was based on the Finite Element Method and generated using the commercial FE package ABAQUS. For this purpose, two types of models were developed as shown in Figure 9: (i) for mother-crack path and (ii) for daughter-crack path. Plane stress assumptions state was adopted in both models. The geometry definition of the considered specimens was generated according to the dimension and shapes defined in the experimental work. The material properties considered henceforth were: Young's Modulus 3.79 GPa and Poisson's ratio 0.37. For the discretization of both models, finite element meshes constituted by eight node plane stress quadratic elements (CPS8) were used, using the quarter-point isoparametric finite elements around the crack tip. The fracture mechanics parameters characterising crack propagation, i.e. Stress Intensity Factors (SIFs) and Energy Release Rate components (ERRs), were computed for each given crack tip position by the *J-Integral* that is a built-in function of ABAQUS. A uniform distributed tensile loading was applied at the outer extremes of the specimens.

The mother-crack model was generated by considering 2 *Parts* separated by the interface, where the interaction between the two parts was modeled using *Tie* option, whereas the daughter-crack model was generated with only 1 *Part*.

In the first model, a partition of the geometry along the horizontal central line was used to model the mother-crack path. The elements on both sides of this discontinuity were separated from each other, i.e. they shared nodes except for the crack faces, where separated nodes on elements were defined. In the second model, we simplified the geometry by considering only one half of the specimen, as is depicted in Figure 9. Then, we propagated the crack along the interface through untying the corresponding FE nodes, similarly as done in the first model.

3.2. Numerical results

The evolution of the SIF k_I , for the straight propagation of the mother crack in mode I, is shown in Figure 10. For the sake of accuracy check, the present computational results were compared with the classical approximations by [50, 51], see Section Appendix A.1 for details. This comparison shows an excellent agreement between the results obtained by both the computational model and the existing benchmark approximations.

In view of the results shown in Figure 10, as expected, the SIF k_I progressively increases with respect to the crack length, which is a necessary condition for an unstable crack growth in a homogeneous material, i.e. without considering any material interfaces.

When the mother crack deflects at the interface, the SIFs evolution changes drastically. Figure 11 shows the SIFs as a function of the crack length when the daughter (interface) cracks propagate along the concave curved path with 25 mm curvature radius. The SIFs computed are compared with their limit values for the daughter crack of vanishing-length kinked by 90° angle obtained from the semianalytical solution deduced in [52], see the expressions reported in Appendix A.2. Noteworthy, it was recently shown in [53] (see Figure 2 therein), that the limit values of SIFs for the vanishing-length daughter cracks are quite close for the symmetrically branched crack and for the kinked crack by angle 90° . As can be observed in Figure 11 the computational results are fully consistent with the semianalytical estimates.

It should be mentioned that for large interface cracks, in the case of concave interface, some overlapping of crack faces may appear, indicated by negative values of SIF k_I (not shown explicitly in Figure 11), which would predict contact between crack faces, not considered in the present computational model. Nevertheless, this will have no influence on the computational-model predictions, due to the fact that the interface cracks that typically kinking out towards the other specimen part would happen for a shorter interface crack length. This statement is based on the experimental observations obtained from our tests.

The observed relevant reduction of the SIFs by increasing the crack length implies a stable crack growth. Moreover, the mode II tends to become the predominant fracture mode. In engineering materials, mode-II crack propagation criteria generally involve higher fracture toughness in comparison to

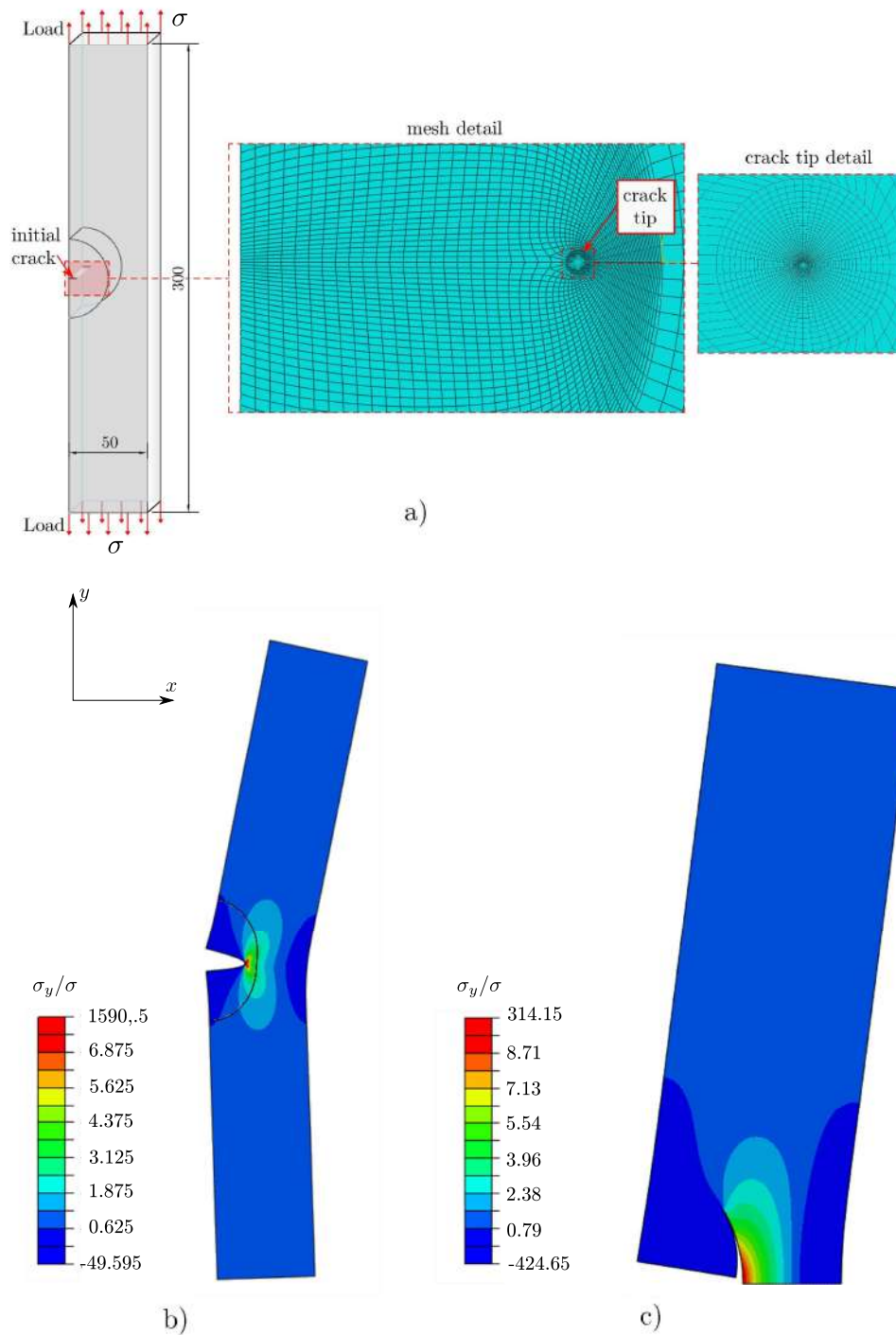


Figure 9: Details of the computational model a) Schematic, b) Results for a mother-crack model c) Results for a daughter-crack model.

mode-I. Therefore, the above results likely imply higher load-carrying capacities of the concave-interface configurations.

In order to evaluate the influence of the curvature radii of the weak interface, the ERR was computed for the different configurations, see Figure 12. For the sake of comparison, the ERR for the mother crack growing straight up to the interface is also reported. Note that the represented crack length corresponds

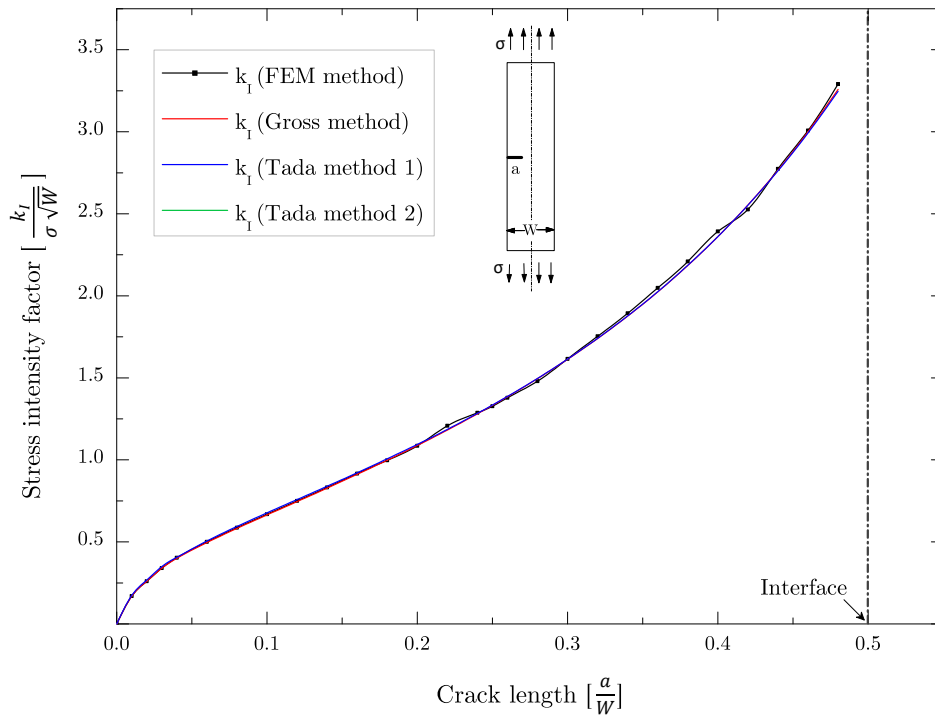


Figure 10: Mode I SIF as a function of the crack length when the mother crack grows straight. Comparison between the results by the computational model and the approximations of the single edge notch test specimen taken from handbooks.

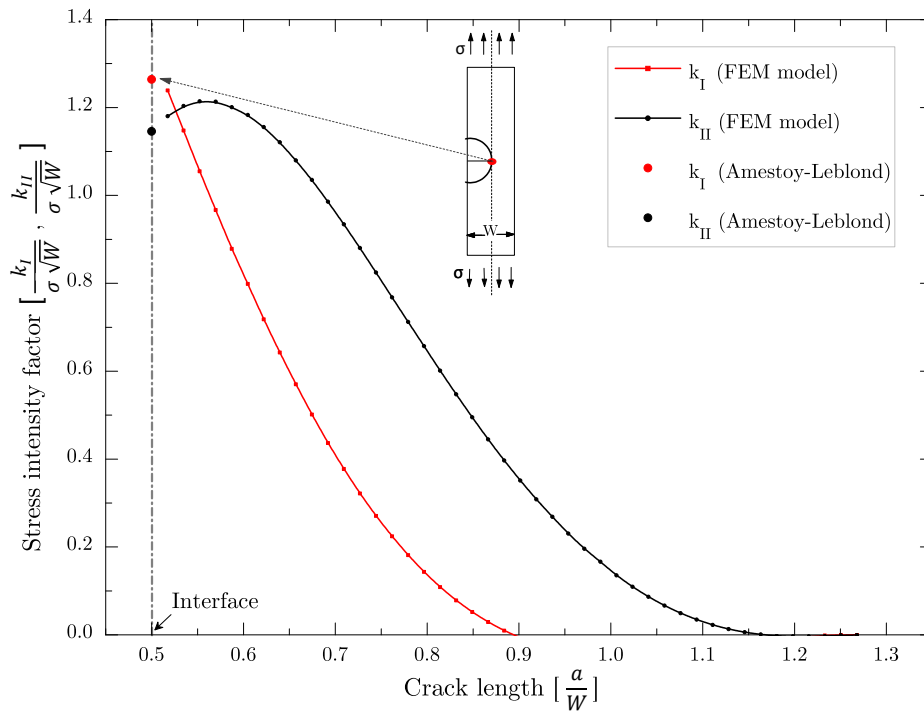


Figure 11: SIFs as a function of the crack length when the daughter cracks grow along the interface for the concave interface with 25 mm radius.

to the sum of the length of the straight crack (mother crack) plus the length of the curved one (one daughter crack).

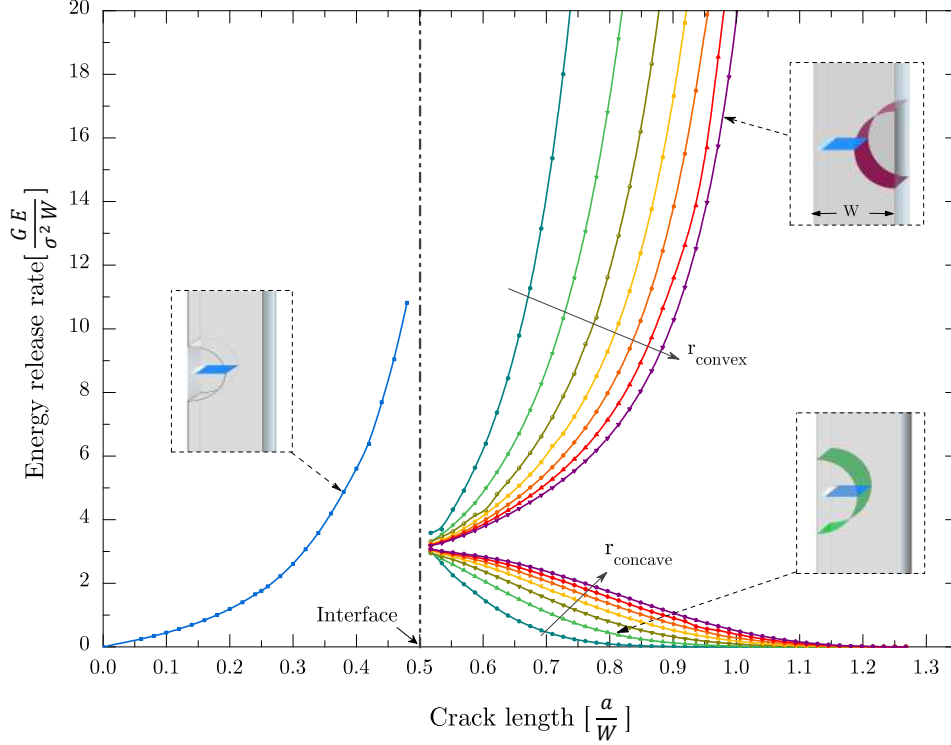


Figure 12: ERR as a function of the crack length, for different potential crack paths.

The results in Figure 12 quantitatively clarify the role of the convexity of the weak interface. For convex interfaces, the ERR is strongly increasing, predicting an unstable crack growth. On the other hand, for concave interfaces, the estimations with regard to the ERR features a decreasing evolution, this fact being related to a stable crack growth. The curvature radius has also a quantitative influence on the ERR behaviour. The general tendency is that a small curvature radius amplifies the effect of the convexity or concavity of the weak interface. Thus, it can be stated that the differences with respect to the ERRs estimations for convex and concave interfaces between two configurations are larger for smaller curvature radius than those corresponding to larger curvature radii.

4. Discussion and interpretation of results

The experimental results can be interpreted thanks to the fracture mechanics data extracted from the computational models.

The propagation of the mother crack up to meeting the interface took place under mode I, and, as usual, it occurred when the corresponding ERR reached the fracture toughness of the bulk. Since the ERR increased with the crack length, the mother crack growth followed an unstable process. When the crack met the interface, its crack path was dictated by the mismatch in the fracture toughness of the bulk and of the interface, that can be assessed by the ratio $G_c^{(i)}/G_c^{(b)}$, as for a straight interface, plus also by the role of the interface curvature, which is an aspect not included in previous theoretical LFM formulations.

For very tough interfaces, it is likely that the mother crack simply penetrates across the interface in a straight manner, because the ERR is higher if the crack goes straight than if the crack deflects at the interface. However, the experiments revealed that the mother crack deflected at the interface, see Table 1, which is a behaviour typical for a weak interface. From a quantitative standpoint, the debonding event along the interface becomes the actual crack path if the ratio between the energy release rate for

the propagation in the bulk and its fracture toughness, $G_c^{(b)}/G_c^{(b)}$, is lower than the ratio between the energy release rate for double deflection and the interface fracture toughness, $G_c^{(i)}/G_c^{(i)}$. From the present experimental results, single deflection was not observed.

Afterwards, along the deviated crack path, further competition between debonding and penetration into the second material layer takes place, depending on the interface curvature. In particular, for convex interfaces, the crack growth of the daughter debonding cracks is unstable since the corresponding ERR is a monotonically increasing with the crack length. On the other hand, for concave interfaces, the ERR is progressively decreasing with the progress of crack propagation. At a certain point, crack arrest or penetration can become favourable over further debonding.

Although it is not an easy task to characterize the interface toughness from experiments, its qualitative identification can be achieved based on the above concepts by re-scaling the ERR for the mother crack and for the daughter cracks by the factor $G_c/G_c^{(b)}$, where G_c is given by $G_c^{(b)}$ for the mother crack and it corresponds to $G_c^{(i)}$ for the interface. A possible re-scaled plot that would be consistent with the experimental evidences is shown in Figure 13 by considering $G_c^{(i)}/G_c^{(b)} = 1/5$, i.e., for an interface five times weaker than the bulk.

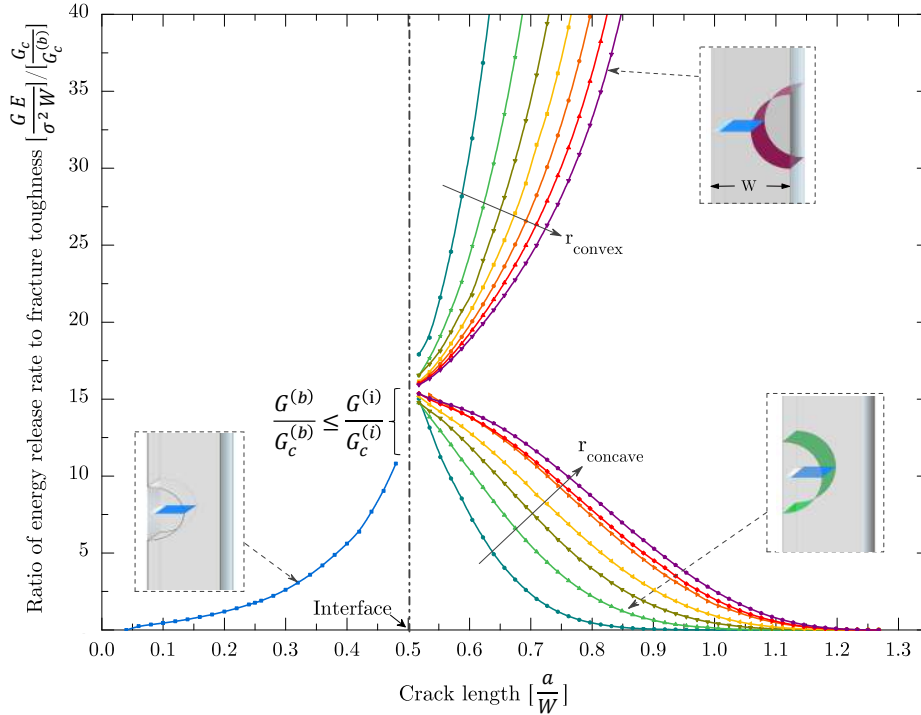


Figure 13: Ratio between the ERRs and $G_c/G_c^{(b)}$, where G_c is given by $G_c^{(b)}$ for the mother crack and it corresponds to $G_c^{(i)}$ for the interface.

According to Figure 13, the radius of curvature of the interface had also an important influence on the crack arrest in concave interfaces. Smaller curvature radii imply lower $G_c^{(i)}$, thus smaller radii favour the occurrence of crack arrest. This protective phenomenon delays kinking out of the interface towards the bulk, and subsequently the final failure of the specimen.

5. Concluding remarks

The experimental evidences presented here originally investigated the phenomenon of crack growth in brittle materials with the presence of weak curved interfaces. The current results showed that it is possible to stop/deviate the unstable crack advancement by means of introducing a concave weak interfaces with a sufficiently small radius of curvature. In contrast to alternative strategies for the design of crack arresters,

the current concept does not imply adding mass to the structure or holes to deviate the crack paths, which is a remarkable advantage in certain industries where minimization of structural weight is a priority and where the overall structural integrity is a major concern. Moreover, if the strategy is well undertaken, it does not imply necessarily either a reduction of stiffness or the introduction of stress concentrations.

The experimental results were interpreted with the help of FEM computational model of the system incorporating LEFM capabilities. The energy release rate (ERR) extracted from the computations satisfactorily agreed with well established crack growth criteria at interfaces [8] and with respect semi-analytical formulations [52]. Consequently, these models provided a suitable methodology to interpret the experimental trends in terms of crack path and its stability, and also to qualitatively identify the interface fracture toughness.

Both experimental results and computational predictions agree on the fact that the concave weak interfaces are able to arrest the unstable crack growth. The final failure of the whole specimen can occur for a load much higher than that required for the propagation of the initial mother crack, thus significantly improving the damage tolerance of the specimen.

The results presented here, in particular in what concerns the computational analysis, are illustrating the crack arrest strategy proposed. Further quantitative analyses are indeed necessary in order to investigate other material configurations depending on the interface fracture toughness and also bi-material configurations, being a matter beyond the scope of the current study. From the experimental point of view, the proposed strategy based on material testing combined with photo-elasticity and digital image correlation acquired in real time with a fast digital camera has been found suitable for the present study where the loading rate was sufficiently low. Additional improvements can be requested to test the specimens also in a full dynamic scenario, up to very high strain rates, which is a topic that would deserve a specific attention.

Acknowledgements

The authors would like to express their gratitude to Professor Davide Bigoni (Universita di Trento, Trento, Italy) for stimulating this research. This investigation was supported by the Spanish Ministry of Economy and Competitiveness and European Regional Development Fund (Project MAT2015-71036-P, UNSE 15-CE-3581), the Junta de Andalucía and the European Social Fund (Programa de Garantía Juvenil 2017), and the Spanish Ministry of Science, Innovation and Universities and European Regional Development Fund (Project PGC2018-099197-B-I00). MP would like to acknowledge the support from the Italian Ministry of Education, University and Research to the Research Project of Relevant National Interest (PRIN-2017) XFAST-SIMS: Extra-fast and accurate simulation of complex structural systems.

Appendix A. Expressions used for verification purposes of the ERR

Appendix A.1. Single edge notch

For single-edge-notched tensile specimen with width b with a crack with length a , open to the left free boundary of the plate, and with uniform tension σ , applied across the upper and lower boundaries of the plate (boundaries parallel to the crack), the value of the Stress Intensity Factor can be approximated by:

$$k_I = \sigma^2 + \sqrt{\pi a} F(a/b) \quad (\text{A.1})$$

where $F(a/b)$ is:

- [50]:

$$F(a/b) = 1.122 - 0.231(a/b) + 10.550(a/b)^2 - 21.710(a/b)^3 + 30.382(a/b)^4 \quad (\text{A.2})$$

with accuracy of 0.5% for $a/b \leq 0.6$.

- [51]:

$$F(a/b) = 0.265(1 - a/b)^4 + \frac{0.857 + 0.265a/b}{(1 - a/b)^{3/2}} \quad (\text{A.3})$$

with accuracy better than 1% for $a/b < 0.2$, and 0.5% for $a/b \geq 0.2$.

- [51]

$$F(a/b) = \sqrt{\frac{2b}{\pi a} \tan \frac{\pi a}{2b} \frac{0.752 + 2.02(a/b) + 0.37(1 - \sin \frac{\pi a}{2b})^3}{\cos \frac{\pi a}{2b}}} \quad (\text{A.4})$$

with accuracy of 0.5% for any a/b .

Appendix A.2. Stress intensity factors just after the kink

According to [52, 54], in plane situation, the stress intensity factor of a kinked crack just after the kink k_p^* , i.e. in the limit when the kink length tends to zero, can be expressed as a function of the stress intensity factor just before the kink, K_q , and the kink angle $m\pi$ (expressed in radians):

$$k_p^* = F_{pq}(m)K_q \quad (\text{A.5})$$

where:

$$F_{11}(m) = 1 - \frac{3\pi^2}{8}m^2 + (\pi^2 - \frac{5\pi^4}{128})m^4 + (\frac{\pi^2}{9} - \frac{11\pi^4}{72} + \frac{119\pi^6}{15360})m^6 + 5.07790m^8 - 2.88312m^{10} - 0.0925m^{12} + 2.996m^{14} - 4.059m^{16} + 1.63m^{18} + 4.1m^{20} \quad (\text{A.6})$$

$$F_{22}(m) = 1 - (4 + \frac{3\pi^2}{8})m^2 + (\frac{8}{3} + \frac{29\pi^2}{18} - \frac{5\pi^4}{128})m^4 + (-\frac{32}{15} - \frac{4\pi^2}{9} - \frac{1159\pi^4}{7200} + \frac{119\pi^6}{15360})m^6 + 10.58254m^8 - 4.78511m^{10} - 1.8804m^{12} + 7.280m^{14} - 7.591m^{16} + 0.25m^{18} + 12.5m^{20} \quad (\text{A.7})$$

$$F_{12}(m) = -\frac{3\pi}{2}m + (\frac{10\pi}{3} + \frac{\pi^3}{16})m^3 + (-2\pi - \frac{133\pi^3}{180} + \frac{59\pi^5}{1280})m^5 + 12.313906m^7 - 7.32433m^9 + 1.5793m^{11} + 4.0216m^{13} - 6.915m^{15} + 4.21m^{17} + 4.56m^{19} \quad (\text{A.8})$$

$$F_{21}(m) = \frac{\pi}{2}m - (\frac{4\pi}{3} + \frac{\pi^3}{48})m^3 + (-\frac{2\pi}{3} + \frac{13\pi^3}{30} - \frac{59\pi^5}{3840})m^5 - 6.176023m^7 + 4.44112m^9 - 1.5340m^{11} - 2.0700m^{13} + 4.684m^{15} - 3.95m^{17} - 1.32m^{19} \quad (\text{A.9})$$

References

References

- [1] D.F.O. Braga, S.M.O. Tavares, L.F.M. Da Silva, P.M.G.P. Moreira, and P.M.S.T. De Castro. Advanced design for lightweight structures: Review and prospects. *Progress in Aerospace Sciences*, 69:29–39, 2014.
- [2] H. Gao. Application of fracture mechanics concepts to hierarchical biomechanics of bone and bone-like materials. *International Journal of Fracture*, 138:101–137, 2006.
- [3] H. Gao, B. Ji, I.L. Jaeger, E. Arzt, and P. Fratzl. Materials become insensitive to flaws at nanoscale: lessons from nature. *Proc.Natl.Acad.Sci.*, 100:5597–5600, 2003.
- [4] H. Gao, B. Ji, M.J. Buehler, and H. Yao. Flaw tolerant bulk and surface nanostructures of biological systems. *Mech. Chem. Biosyst.*, 1:37–52, 2004.
- [5] M. Paggi and P. Wriggers. Stiffness and strength of hierarchical polycrystalline materials with imperfect interfaces. *Journal of the Mechanics and Physics of Solids*, 60(4):557–572, 2012.
- [6] M. R. Lena, J. C. Klug, and C. T. Sun. Composite Patches as Reinforcements and Crack Arrestors in Aircraft Structures. *Journal of Aircraft*, 35(2):318–323, 2008.

- [7] Francis S. Somerville. United state patent: Method of applying a crack arrestor, May 1982.
- [8] Ming-Yuan He and John W Hutchinson. Crack deflection at an interface between dissimilar elastic materials. *International Journal of Solids and Structures*, 25(9):1053–1067, 1989.
- [9] J.W. Hutchinson and Z. Suo. Mixed mode cracking in layered materials. *Advances in Applied Mechanics*, 29:63–191, 1992.
- [10] J Cook and J.E. Gordon. A mechanism for the control of crack propagation in all-brittle systems. *Proceedings of the Royal Society A: Mathematical, Physical and Engineering Sciences*, 282(1391):508–520, 1964.
- [11] C.E. Inglis. Stress in a plate due to the presence of cracks and sharp corners. *Transactions on the Institute of Naval Architects*, 55:219–241, 1913.
- [12] D. Leguillon, C. Lacroix, and E. Martin. Interface debonding ahead of a primary crack. *Journal of the Mechanics and Physics of Solids*, 48(10):2137–2161, 2000.
- [13] P. A. Martin. The spherical-cap crack revisited. *International Journal of Solids and Structures*, 38(26-27):4759–4776, 2001.
- [14] E. Martin, B. Poitou, D. Leguillon, and J. M. Gatt. Competition between deflection and penetration at an interface in the vicinity of a main crack. *International Journal of Fracture*, 151(2):247–268, 2008.
- [15] G. I. Barenblatt. The mathematical theory of equilibrium cracks in brittle fracture. *Advances in Applied Mechanics*, 7:55–129, 1962.
- [16] D. S. Dugdale. Yielding of steel sheets containing slits. *Journal of the Mechanics and Physics of Solids*, 8(2):100–104, 1960.
- [17] JP Parmigiani and MD Thouless. The roles of toughness and cohesive strength on crack deflection at interfaces. *Journal of the Mechanics and Physics of Solids*, 54(2):266–287, 2006.
- [18] M Paggi and P Wriggers. Stiffness and strength of hierarchical polycrystalline materials with imperfect interfaces. *Journal of the Mechanics and Physics of Solids*, 60(4):557–572, 2012.
- [19] X-P Xu and A Needleman. Numerical simulations of fast crack growth in brittle solids. *Journal of the Mechanics and Physics of Solids*, 42(9):1397–1434, 1994.
- [20] B Bourdin, GA Francfort, and J-J Marigo. The variational approach to fracture. *Journal of elasticity*, 91(1):5–148, 2008.
- [21] C Miehe, M Hofacker, and F Welschinger. A phase field model for rate-independent crack propagation: Robust algorithmic implementation based on operator splits. *Computer Methods in Applied Mechanics and Engineering*, 199(45):2765–2778, 2010.
- [22] GA Francfort and J-J Marigo. Revisiting brittle fracture as an energy minimization problem. *Journal of the Mechanics and Physics of Solids*, 46(8):1319–1342, 1998.
- [23] M Paggi and J Reinoso. Revisiting the problem of a crack impinging on an interface: a modeling framework for the interaction between the phase field approach for brittle fracture and the interface cohesive zone model. *Computer Methods in Applied Mechanics and Engineering*, 321:145–172, 2017.
- [24] V. Carollo, J. Reinoso, and M. Paggi. Modeling complex crack paths in ceramic laminates: A novel variational framework combining the phase field method of fracture and the cohesive zone model. *Journal of the European Ceramic Society*, 38(8):2994 – 3003, 2018. Cermodel 2017: Modelling and Simulation Meet Innovation in Ceramics Technology.
- [25] V Carollo, J Reinoso, and M Paggi. A 3d finite strain model for intralayer and interlayer crack simulation coupling the phase field approach and cohesive zone model. *Composite Structures*, 182:636–651, 2017.
- [26] M Paggi, M Corrado, and J Reinoso. Fracture of solar-grade anisotropic polycrystalline silicon: A combined phase field–cohesive zone model approach. *Computer Methods in Applied Mechanics and Engineering*, 330:123–148, 2018.
- [27] I. G. García, M. Paggi, and V. Mantič. Fiber-size effects on the onset of fiber-matrix debonding under transverse tension: A comparison between cohesive zone and finite fracture mechanics models. *Engineering Fracture Mechanics*, 115:96–110, 2014.
- [28] D. Leguillon. Strength or toughness? A criterion for crack onset at a notch. *European Journal of Mechanics and Solids*, 21(1):61–72, 2002.
- [29] E. Martin, D. Leguillon, and N. Carrère. A coupled strength and toughness criterion for the prediction of the open hole tensile strength of a composite plate. *International Journal of Solids and Structures*, 49(26):3915–3922, 2012.
- [30] P. Weissgraeber and W. Becker. A new finite fracture mechanics approach for assessing the strength of bonded lap joints. *Key Engineering Materials*, 471-472:1075–1080, 2011.
- [31] D. Leguillon. A simple model of thermal crack pattern formation using the coupled criterion. *Comptes Rendus Mécanique*, 341(6):538–546, 2013.
- [32] I. G. García, V. Mantič, and A. Blázquez. The effect of residual thermal stresses on transverse cracking in cross-ply laminates. An application of the Coupled Criterion of the Finite Fracture Mechanics. *International Journal of Fracture*, 211:61–74, 2018.
- [33] V. Mantič and I. G. García. Crack onset and growth at the fibre-matrix interface under a remote biaxial transverse load. Application of a coupled stress and energy criterion. *International Journal of Solids and Structures*, 49(17):2273–2290, 2012.
- [34] I. G. García, V. Mantič, A. Blázquez, and F. París. Transverse crack onset and growth in cross-ply [0/90]_s laminates under tension. Application of a coupled stress and energy criterion. *International Journal of Solids and Structures*, 51(23-24):3844–3856, 2014.
- [35] Ares J Rosakis, Omprakash Samudrala, Raman P Singh, and A Shukla. Intersonic crack propagation in bimaterial systems. *Journal of the Mechanics and Physics of Solids*, 46(10):1789 – 1814, 1998.
- [36] V.B. Chalivendra and A.J. Rosakis. Interaction of dynamic mode-I cracks with inclined interfaces. *Engineering Fracture Mechanics*, 75(8):2385 – 2397, 2008.
- [37] Mahabub Alam, John P. Parmigiani, and Jamie J. Kruzic. An experimental assessment of methods to predict crack

- deflection at an interface. *Engineering Fracture Mechanics*, 181:116 – 129, 2017.
- [38] Balamurugan M. Sundaram and Hareesh V. Tippur. Dynamics of crack penetration vs. branching at a weak interface: An experimental study. *Journal of the Mechanics and Physics of Solids*, 96:312 – 332, 2016.
- [39] Balamurugan M. Sundaram and Hareesh V. Tippur. Dynamic fracture of soda-lime glass: A full-field optical investigation of crack initiation, propagation and branching. *Journal of the Mechanics and Physics of Solids*, 120:132 – 153, 2018. Special issue in honor of Ares J. Rosakis on the occasion of his 60th birthday.
- [40] F.A. Cordisco, P.D. Zavattieri, L.G. Hector Jr, and B.L. Carlson. Mode I fracture along adhesively bonded sinusoidal interfaces. *International Journal of Solids and Structures*, 83:45–64, 2016.
- [41] L. García-Guzmán, L. Távara, J. Reinoso, J. Justo, and F. París. Fracture resistance of 3D printed adhesively bonded DCB composite specimens using structured interfaces: Experimental and theoretical study. *Composites Structures*, 185:537–548, 2017.
- [42] K. Bertoldi, D. Bigoni, and W.J. Drugan. Structural interfaces in linear elasticity. part i: Nonlocality and gradient approximations. *Journal of the Mechanics and Physics of Solids*, 55(1):1 – 34, 2007.
- [43] D. Bigoni and A.B. Movchan. Statics and dynamics of structural interfaces in elasticity. *International Journal of Solids and Structures*, 39(19):4843 – 4865, 2002.
- [44] B.M. Sundaram and H.V. Tippur. Dynamics of crack penetration vs. branching at a weak interface: An experimental study. *Journal of the Mechanics and Physics of Solids*, 96:312–332, 2016.
- [45] G. Noselli, F. Dal Corso, and D. Bigoni. The stress intensity near a stiffener disclosed by photoelasticity. *International Journal of Fracture*, 166:91–103, 2010.
- [46] F. Dal Corso, D. Bigoni, and M. Gei. The stress concentration near a rigid line inclusion in a prestressed, elastic material. part i.: Full-field solution and asymptotics. *Journal of the Mechanics and Physics of Solids*, 56:815–838, 2008.
- [47] D. Misseroni, F. Dal Corso, S. Shahzad, and D. Bigoni. Stress concentration near stiff inclusions: Validation of rigid inclusion model and boundary layers by means of photoelasticity. *Engineering Fracture Mechanics*, 121–122:87–97, 2014.
- [48] ASTM. ASTM D 5045-99: Standard Test Method for Plane-Strain Fracture Toughness and Strain Energy Release Rate of Plastic Materials, 2007.
- [49] Afonso Leite, Vladislav Mantič, and Federico París. Crack Onset in a Polymer Matrix With Open-Hole Configuration and Viscoelastic Behavior. Application of the finite fracture mechanics compued criterion. In *Proc. of the 20th International Conference on Composite Materials (ECCM, Sevilla, Spain, June 2014)*, 2014.
- [50] Stress-Intensity Factors for a Single-Edge-Notch Tension Specimen by Boundary Collocation of a Stress Function. Mobile Systems IV. Technical report, NASA Technical note D-2395, 1964.
- [51] H. Tada, P.C. Paris, and G.R. Irwin. *The stress analysis of cracks handbook*. John Wiley & Sons, London, 2000.
- [52] J. B. Leblond. Crack paths in plane situations-I. General form of the expansion of the stress intensity factors. *International Journal of Solids and Structures*, 25(1):1311–1325, 1989.
- [53] E. Katzav, M. Adda-Bedia, and R. Arias. Theory of dynamic crack branching in brittle materials. *International Journal of Fracture*, 143(3):245–271, 2007.
- [54] M. Amestoy and J.B. Leblond. Crack paths in plane situationsii. detailed form of the expansion of the stress intensity factors. *International Journal of Solids and Structures*, 29(4):465 – 501, 1992.